

## In-insect synthesis of oxygen-doped molecular nanocarbons

Atsushi Usami<sup>†,‡,\*||</sup>, Hideya Kono<sup>∇||</sup>, Vic Austen<sup>∇||</sup>, Quan Manh Phung<sup>‡,∇</sup>, Hiroki Shudo<sup>∇</sup>, Tomoki Kato<sup>∇</sup>, Hayato Yamada<sup>∇,§</sup>, Akiko Yagi<sup>‡,∇</sup>, Kazuma Amaike<sup>†,⊥</sup>, Kazuhiro J. Fujimoto<sup>‡,∇,\*</sup>, Takeshi Yanai<sup>‡,∇,\*</sup>, Kenichiro Itami<sup>‡,¶,\*</sup>

<sup>†</sup> Institute for Advanced Research, Nagoya University, Chikusa, Nagoya 464-8602, Japan.

<sup>‡</sup> Institute of Transformative Bio-Molecules (WPI-ITbM), Nagoya University, Chikusa, Nagoya 464-8602, Japan.

<sup>∇</sup> Department of Chemistry, Graduate School of Science, Nagoya University, Chikusa, Nagoya 464-8602, Japan.

<sup>§</sup> Integrated Research Consortium on Chemical Sciences, Nagoya University, Chikusa, Nagoya 464-8602, Japan.

<sup>⊥</sup> Research Center for Materials Science, Nagoya University, Chikusa, Nagoya 464-8602, Japan.

<sup>¶</sup> Molecule Creation Laboratory, Cluster for Pioneering Research, RIKEN, Wako, Saitama 351-0198, Japan.

<sup>||</sup> These authors contributed equally to this work.

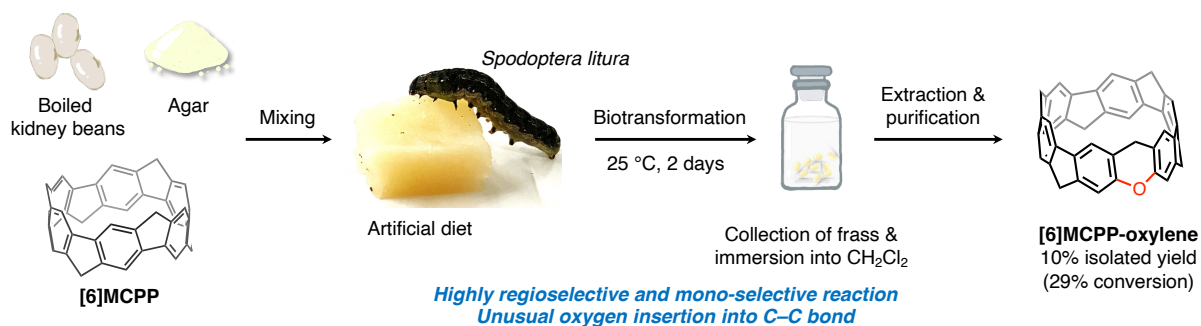
\*Corresponding authors. Email: [usami.atsushi.y5@f.mail.nagoya-u.ac.jp](mailto:usami.atsushi.y5@f.mail.nagoya-u.ac.jp), [fujimotok@chem.nagoya-u.ac.jp](mailto:fujimotok@chem.nagoya-u.ac.jp), [yanait@chem.nagoya-u.ac.jp](mailto:yanait@chem.nagoya-u.ac.jp), [kenichiro.itami@riken.jp](mailto:kenichiro.itami@riken.jp)

**KEYWORDS:** Molecular nanocarbon, Insects, Biotransformation, Molecular dynamics simulation, quantum chemical simulation

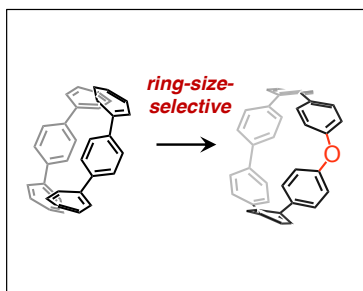
## ABSTRACT:

Many functional molecules and materials have been produced using flask chemical reactions. Meanwhile, individual organisms, such as insects, have the potential to serve as natural, high-density cultivation equipment with multiple enzymes capable of complex reactions. However, research in this area has focused on the composition and reactivity of enzymes involved in biological reactions. Here, we report a unique “in-insect” unnatural product synthesis. Biotransformation using insect xenobiotic metabolism can selectively transform belt- and ring-shaped molecular nanocarbons into other difficult-to-prepare functional oxygen-doped derivatives. Cytochrome P450 variants are most likely the enzymes responsible for this reaction. Molecular dynamics simulations and quantum chemical calculations indicated a possible mode of substrate incorporation into the enzyme and an unconventional mechanism of direct oxygen insertion into carbon–carbon bonds.

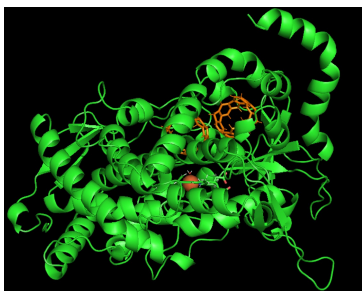
### Discovery of in-insect transformation of belt-shaped molecular nanocarbons



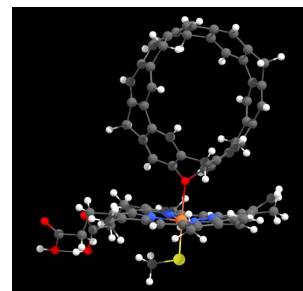
**Cycloparaphenylenes also undergo ring-size-selective oxygen doping.**



**Cytochrome P450 variants are most likely enzymes responsible.**



**Implication of unconventional direct oxygen-insertion mechanism.**



## INTRODUCTION

Functional molecules integral to our daily lives, such as pharmaceuticals, optoelectronic materials, and polymers, have been produced through in-flask chemical reactions utilizing precisely designed reagents and catalysts. Meanwhile, natural products secreted by organisms are often difficult to synthesize using conventional in-flask reactions. One major factor contributing to this challenge is the ability of the organism to adapt to the changing environment and perform complex reactions as efficiently and accurately as high-density culture devices.<sup>1–3</sup> Notably, insects have developed highly effective detoxification systems and control mechanisms against xenobiotics, such as plant secondary metabolites and pesticides.<sup>4</sup> However, research has thus far primarily focused on the composition and reactivity of enzymes participating in biological reactions, with no examples demonstrating active utilization for the production of unnatural functional molecules through xenobiotic metabolism.

The overall aim of this study was to hijack the insects' xenobiotics metabolism for creating new functional organic materials. We now report a unique “in-insect” unnatural product synthesis where biotransformation using insect xenobiotic metabolism can selectively functionalize specific molecular nanocarbons, to yield otherwise difficult-to-make and functional molecular nanocarbons.<sup>5</sup> Molecular nanocarbons, such as C<sub>60</sub> fullerene,<sup>6</sup> cycloparaphenylenes (CPPs),<sup>7–11</sup> carbon nanobelts (ultrashort armchair-type carbon nanotubes),<sup>12–19</sup> methylene-bridged CPPs (MCPPs: a segment structure of haeckelite carbon nanotubes and C<sub>80</sub> fullerene),<sup>20, 21</sup> warped nanographenes,<sup>22–24</sup> and cyclocarbons,<sup>25, 26</sup> have received significant attention in various kinds of research in recent years (Figure 1a).<sup>5</sup> Although considerable progress has been made in this field, bottlenecks exist in the synthesis and functionalization of these molecules. While the functionalization of molecular nanocarbons is crucial for preparing analogs suited for target applications, successful examples are minimal, except for C<sub>60</sub>, mainly because of the limited toolbox for in-flask synthesis. We envision that in-insect synthesis provides significant opportunities as an enabling technology for the preparation of new molecular nanocarbons.

### In-insect transformation of methylene-bridged [6]cycloparaphenylene

We selected methylene-bridged [6]cycloparaphenylene ([6]MCP) as the first molecular nanocarbon substrate in this study because of its rigid and belt-like structure,<sup>20,21</sup> excellent conductivity,<sup>27</sup> and commercial availability.<sup>28</sup> We began by feeding [6]MCP to insects; however, in many cases, they did not survive because of the inherent toxicity of [6]MCP. While searching for durable species, we discovered that the tobacco cutworm *Spodoptera litura* (Lepidoptera, Noctuidae) was suitable for the in-insect functionalization of [6]MCP. *S. litura* is a polyphagous pest that feeds on more than 120 plant species.<sup>29</sup> *S. litura* has a biological life cycle of 35–40 days, and a simple xenobiotic metabolism test (biotransformation) using the oral administration of plant secondary metabolites and pesticides has been established.<sup>30</sup> Moreover, recent genomic studies have reported that *S. litura* possesses approximately twice as many detoxifying enzymes, such as cytochrome P450 (CYPs), carboxylesterase, and glutathione-*S*-transferase, as the monophagous species *Bombyx mori* (domestic silkworm), a known lepidopteran model insect.<sup>31</sup> These aspects of *S. litura* xenobiotic metabolism are likely the reasons for the success of this study.

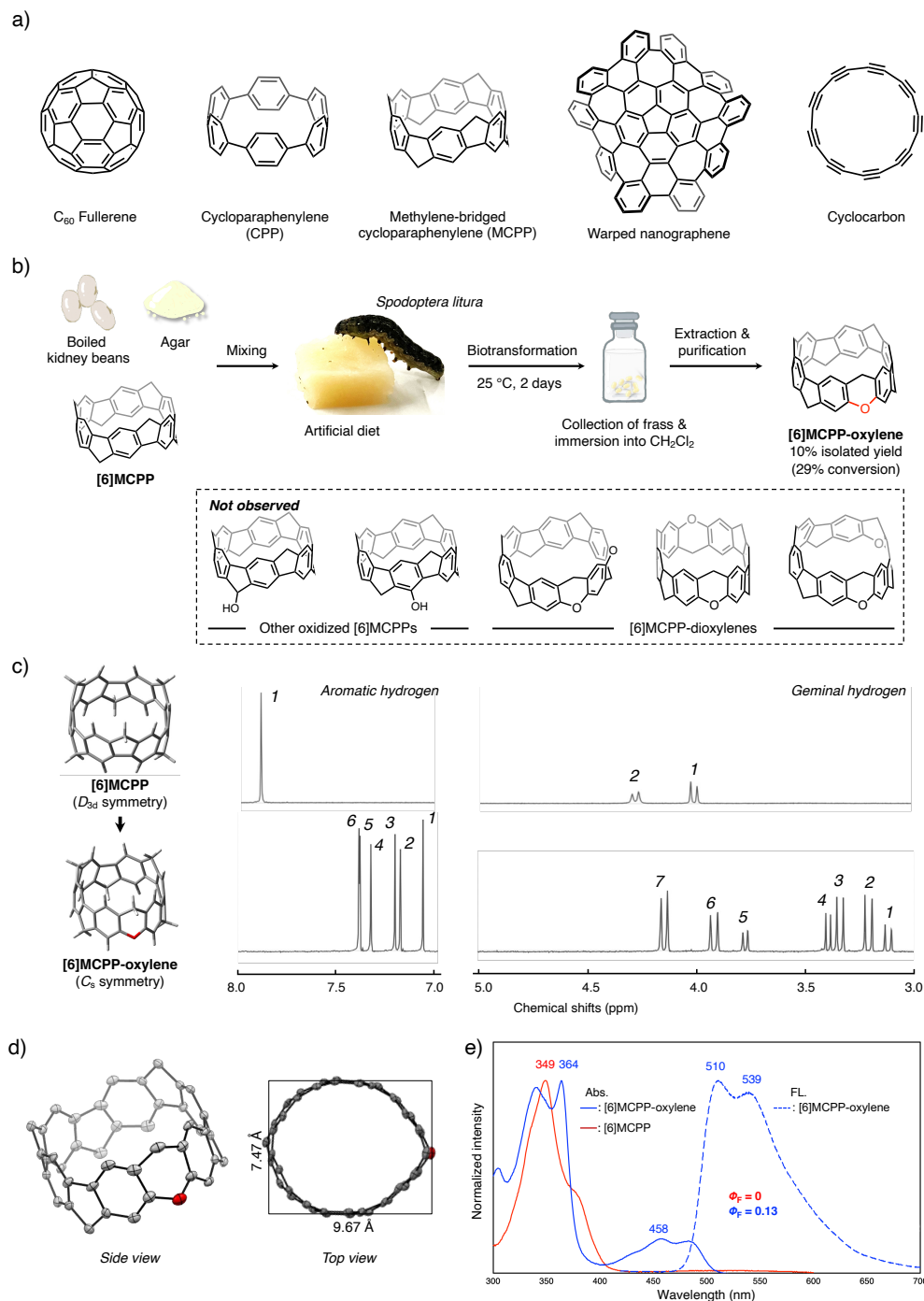


**Figure 1. In-insect transformation of molecular nanocarbons by *Spodoptera litura*.** a) Representative molecular nanocarbons. b) Scheme of the biotransformation. Reaction conditions: The artificial diet consists of boiled kidney beans, agar, water, and molecular nanocarbons. The insects are the fourth- and fifth-instar larvae of *Spodoptera litura*. The frass is collected and immersed in a solvent. The product is purified from the frass extract. c)  $^1H$  NMR spectra of [6]MCPP and [6]MCPP-oxylene. d) Oak Ridge thermal ellipsoid plot (ORTEP) drawing [6]MCPP-oxylene with thermal ellipsoids set to 50% probability. Hydrogen atoms and solvent molecules are omitted for clarity. e) Ultraviolet-visible absorption (solid lines) and fluorescence (dashed line) spectra of the toluene solutions of [6]MCPP and [6]MCPP-oxylene. The fluorescence spectra were measured upon excitation at 360 nm for [6]MCPP-oxylene.

The in-insect functionalization of [6]MCP was conducted as shown in Figure 1b. Groups of 50 larvae were fed an artificial diet containing [6]MCP (200 nmol/larva), boiled kidney beans, and agar for two days.<sup>32</sup> An artificial diet without [6]MCP was administered for an additional day to completely excrete [6]MCP from the body. Fresh frass was collected every 12 hours for 3 days and immersed in CH<sub>2</sub>Cl<sub>2</sub>, followed by extraction. In this crude extract, we identified the presence of one [6]MCP derivative in addition to the remaining unreacted [6]MCP. The sole product formed was found to be an oxygen adduct by MALDI-TOF mass spectrometry; thus, we named this product [6]MCP-oxylene. Through purification by gel permeation chromatography (GPC) and preparative thin-layer chromatography (PTLC), [6]MCP-oxylene was isolated in 9.9 ± 0.4% yield while [6]MCP was recovered in 71.1 ± 18.3% yield. The selectivity (substrate specificity) of this biotransformation is high as [6]MCP-oxylene remains the sole product even when the reaction scale increased 50-fold, and dioxylene products were not observed under any of the conditions we tested. The feeding activity of *S. litura* was affected when the concentration of [6]MCP exceeded 400 nmol/larva. Therefore, [6]MCP concentration of 200 nmol/larva seems to be optimal for this biotransformation and the upper limit at which there was no feeding inhibition of larvae (see Supporting Information for details).

Initially, we assumed that [6]MCP-oxylene was a typical C–H bond hydroxylation product at either the aromatic or benzylic C–H bond of [6]MCP. However, the <sup>1</sup>H-NMR spectrum of [6]MCP-oxylene in CD<sub>2</sub>Cl<sub>2</sub> at 25 °C shows six singlets of aromatic hydrogen atoms and seven doublets of geminal hydrogen atoms (Figure 1c), which does not match with either aromatic or benzylic C–H bond hydroxylation product (Figure 1b). The surprising structure of [6]MCP-oxylene was revealed by single-crystal X-ray crystallography (Figure 1d), in which the oxygen atom was inserted by cleaving the C<sub>phenyl</sub>–C<sub>phenyl</sub> bond on the opposite side of the methylene moiety in the five-membered ring. The highly symmetric belt structure of [6]MCP<sup>20</sup> is significantly altered into an oval shape in [6]MCP-oxylene, exhibiting a short diameter of 7.47 Å and a long diameter of 9.67 Å. In the solid state, [6]MCP-oxylene was found to align and stack to fill the interior of the ring structure, with one molecule tilted at approximately 90° relative to the other (see Supporting Information for details). The optimized structure of [6]MCP-oxylene exhibits C<sub>s</sub> symmetry, which agrees well with its <sup>1</sup>H-NMR spectrum.

The influence of oxygen-doping on the optical properties of the [6]MCP framework can be observed in the UV-vis absorption and fluorescence spectra of [6]MCP-oxylene vs [6]MCP (Figure 1e). The major absorption band of [6]MCP-oxylene was observed at a maximum absorption wavelength (λ<sub>max</sub>) of 364 nm, which is bathochromically shifted compared with that of [6]MCP (349 nm). While [6]MCP shows a weak absorption band within the 450–600 nm wavelength region, [6]MCP-oxylene shows a maximum absorption wavelength of 458 nm and absorption bands in the 400–500 nm range. No fluorescence is observed for [6]MCP, but [6]MCP-oxylene fluoresces at 510 and 539 nm with a fluorescence quantum yield (Φ<sub>F</sub>) of 0.13 at 25 °C in toluene. This simple yet significant alteration in the structure and properties of [6]MCP underscores the power of the present one-shot in-insect transformation as well as the potential of otherwise difficult-to-make [6]MCP-oxylene in various applications.

## Identification of responsible enzymes

In addition to the significance of the product generated, the pathway and mechanism of [6]MCP-oxylene formation are of fundamental interest. To verify whether the oxygen-doping of [6]MCP was derived from intestinal bacteria and/or enzymes within the body, biotransformation

was conducted using intestinal bacteria as the target. However, it was clearly shown that bacteria were not involved in biotransformation (see Supporting Information for details). Next, the effects of [6]MCPD feeding on individual insects were comprehensively analyzed using RNA sequencing to identify enriched Kyoto Encyclopedia of Genes and Genomes (KEGG) and differentially expressed genes (DEGs) pathways. The enriched KEGG analysis is shown in detail in the Supporting Information. The most significant signaling pathway was the intestinal immune network for IgA production. This suggests that the accelerated neutralizing function of [6]MCPD can be attributed to its recognition as a xenobiotic or toxin. The number of expressed genes that increased (red) or decreased (blue) upon feeding [6]MCPD is shown in Figure 2a. In particular, an increase in the gene expression of metabolism-related pathways was observed. Based on the biotransformation pathway (Figure 1b), which involves the insertion of the single oxygen atom into [6]MCPD, we focused on five CYP variants [No. 1, 2, 3, 4, and 5; cytochrome P450 6B2-like isoforms X1 (RefSeq ID; XP\_022824880), X2 (XP\_022824881), X3 (XP\_022824882), X4 (XP\_022824884), and X5 (XP\_022824885)] that were suggested to be involved in xenobiotic metabolism.<sup>31,33</sup> These CYP variants exhibited different levels of gene expression associated with [6]MCPD-feeding, as determined by quantitative reverse transcription-polymerase chain reaction (qRT-PCR) (Figure 2b). These results suggested that at least three CYP variants are involved in biotransformation of [6]MCPD.<sup>31</sup> We then employed an RNA interference (RNAi) technique,<sup>34</sup> in which a small interfering RNA (siRNA) targeting these CYP variants was injected into the hemolymph of *S. litura* larvae (Figure 2c). The siRNA used in this study was designed to knockdown the expression levels of five CYP genes, rather than targeting a specific CYP gene. We examined the expression levels of three CYP variants that were predominantly upregulated by [6]MCPD feeding and the production of [6]MCPD-oxyene. The levels of gene expression for each CYP in *S. litura* fed [6]MCPD after siRNA injection were 20–80% lower than those in injected with siRNA against green fluorescent protein (GFP) as a control, with significant differences in CYP No.3 and CYP No.4 (Figure 2d). The siRNA injection decreased the production yield of [6]MCPD-oxyene to  $4.4 \pm 1.9\%$  (Figure 2e). Therefore, these CYP variants are key enzymes in the biotransformation process. These CYP variants are microsomal cytochrome P450s that bind to the membrane through their N-terminal transmembrane hydrophobic segment, and thus direct purification and functional evaluation of these proteins from insects is challenging with high technical demand. In our longer-term campaign, the enzymatic activities of the individual CYP variants will be elucidated by heterologous expression in hosts such as *Escherichia coli*, yeast, and insect cells with optimized conditions, followed by purification and *in vitro* assays.

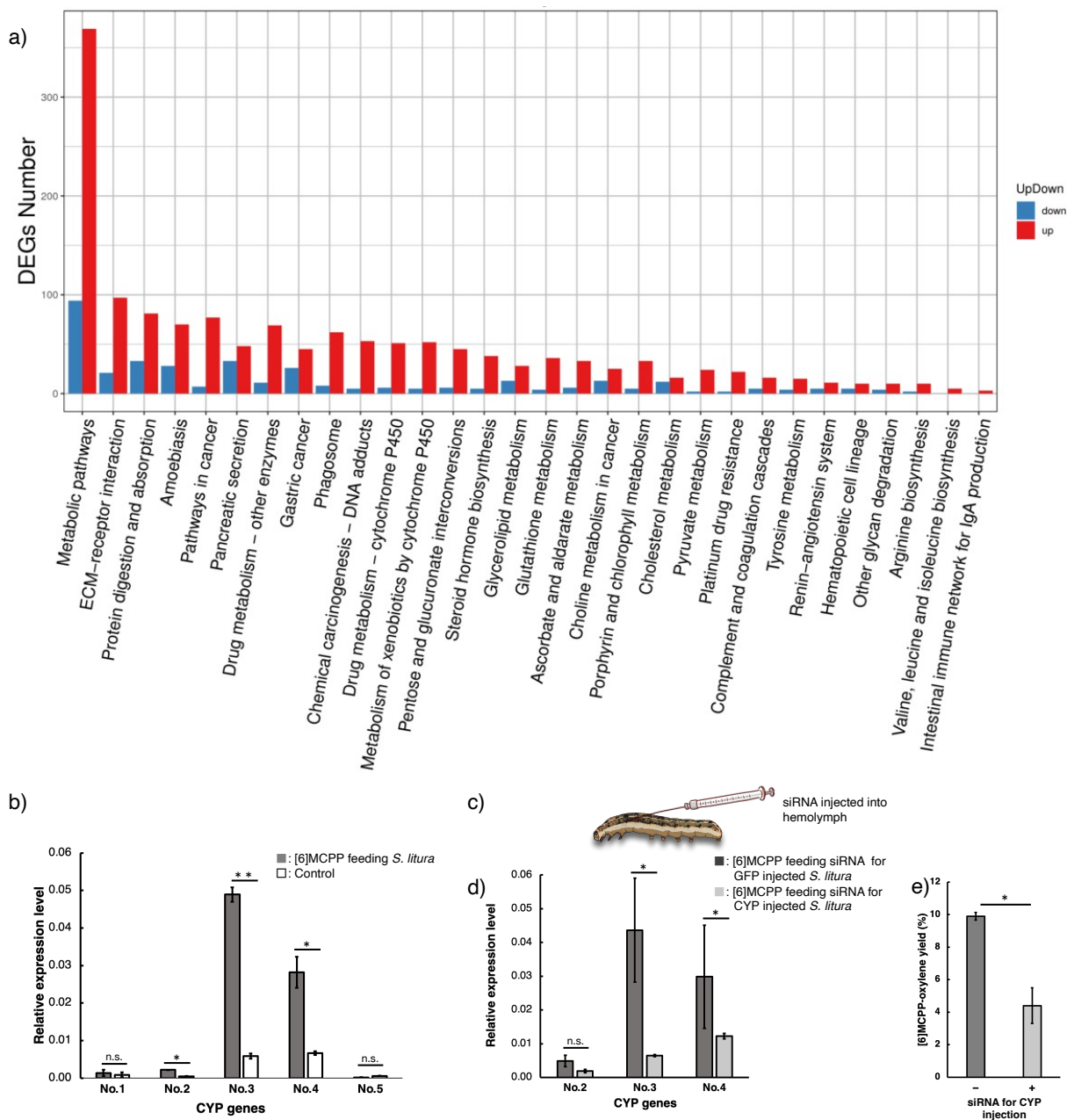


**Figure 2.** Insight of in-insect synthesis of [6]MCCP-oxylene by *Spodoptera litura*. a) Differentially expressed genes (DEGs) analysis of [6]MCCPP-feeding *S. litura*. Up-regulation, red; Down-regulation, blue. b) qRT-PCR of five CYP genes in the midgut of *S. litura* fed [6]MCCPP. The reference gene is EF-1 $\alpha$ . c) Injection of siRNA into the hemolymph. d) qRT-PCR of three CYP genes in the midgut of siRNA-injected *Spodoptera litura* fed [6]MCCPP. e) Biotransformation of MCCPP by siRNA for GFP or CYP injected *S. litura*. (–), *S. litura* with siRNA for GFP injected.; (+), *S. litura* with siRNA for CYP injected. Statistically, significant differences are indicated with their respective  $p$ -values (\* $p < 0.05$ , \*\* $p < 0.01$ , Welch's  $t$ -test). Columns and bars indicate means and standard error of the mean (SEM) from three independent experiments.

## In-insect transformation of cycloparaphenylenes

Having established the in-insect oxygen-doping of [6]MCP, we hypothesized that the *S. litura* mediated reaction can be extended to carbon nanorings, [*n*]cycloparaphenylene ([*n*]CPP).<sup>7-11</sup> Thus, eight carbon nanorings of different ring sizes ([5]CPP to [12]CPP) were used as starting materials and biotransformed by *S. litura* larvae. Interestingly, the biotransformation of CPPs by *S. litura* larvae is a size-selective reaction that proceeds exclusively with [6]CPP (Figure 3a and see Supporting Information for details). In the reaction of [6]CPP under otherwise identical conditions, oxygen-doped [6]CPP ([6]CPP-oxylene) was similarly isolated in  $5.8 \pm 0.9\%$  yield together with unreacted [6]CPP ( $50.0 \pm 17.0\%$ ) from the frass extract. The structure of [6]CPP-oxylene, in which a single oxygen atom is inserted into a C<sub>phenyl</sub>-C<sub>phenyl</sub> bond of the CPP framework, was unequivocally confirmed by single-crystal X-ray crystallography analysis. Similar to the case of [6]MCP-oxylene, the symmetry of the molecules changed from *D*<sub>3d</sub> symmetric ([6]CPP) to *C*<sub>2</sub> symmetric ([6]CPP-oxylene) (Figure 3b, see Supporting Information for details). [6]CPP-oxylene shows a weak absorption band at 400–500 nm, whereas [6]CPP shows a maximum absorption wavelength at 414 nm and absorption bands at 360–480 nm (Figure 3c). This oxygen-doping assists emerging fluorescence properties. While [6]CPP is non-fluorescent, [6]CPP-oxylene exhibits an emission band centered at 524 nm with a quantum efficiency ( $\Phi_F$ ) of 0.26 at 25 °C in toluene. The gene expression levels of the CYP variants exhibited slight variations compared to the biotransformation of [6]MCP, with only CYP No.4 showing a significant difference as shown in Figure 3d. This difference in the expression levels of CYP variants suggests that [6]CPP is more conformationally flexible than [6]MCP, thereby affecting its binding stability to CYPs.

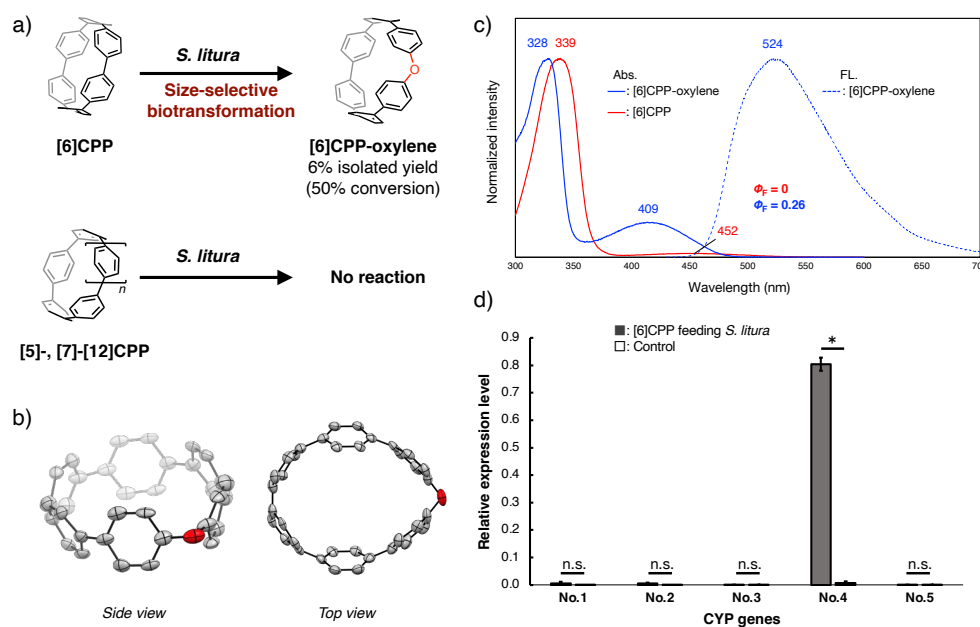


**Figure 3. In-insect transformation of [6]cycloparaphenylene ([6]CPP).** a) In-insect synthesis of [6]CPP-oxylene. b) Oak Ridge thermal ellipsoid plot (ORTEP) drawing [6]CPP-oxylene with thermal ellipsoids set to 50% probability. Hydrogen atoms and solvent molecules are omitted for clarity. c) Ultraviolet-visible absorption (solid lines) and fluorescence (dashed line) spectra of the toluene solutions of [6]CPP and [6]CPP-oxylene. The fluorescence spectra were measured upon excitation at 410 nm for [6]CPP-oxylene. d) qRT-PCR of five CYP genes in the midgut of *Spodoptera litura* fed [6]CPP. The reference gene is EF-1 $\alpha$ . Statistically, significant differences are indicated with their respective *p*-values (*p* < 0.05, Welch's *t*-test). Columns and bars indicate means and SEM from three independent experiments.

## Substrate binding to CYP variants

The mode of substrate incorporation into the CYP variants and the mechanism of oxygen insertion are of significant interest. Thus, we first performed a two-step calculation of the binding affinity between [6]MCPP and the CYP variants. For the calculation, CYP No.3 was selected, because its expression was the most upregulated during the biotransformation of [6]MCPP. First, docking simulations<sup>35</sup> were performed to explore the conformation of [6]MCPP binding to CYP No.3. Given that the three-dimensional structure of CYP No.3 has not been experimentally determined, the structure predicted by AlphaFold2<sup>36</sup> was used in the simulations. Placement of the heme cofactor at the active site of CYP was determined by superposition with a structurally homologous enzyme, human CYP3A4 (PDB ID: 4I3Q).<sup>37</sup> The results of the docking simulations yielded insights into the arrangement of [6]MCPP within CYP No.3. Subsequently, molecular dynamics (MD) simulations were conducted on the obtained [6]MCPP-CYP No.3 complex structure (Movie S1). As illustrated in Figure 4a, the results demonstrated the sustained stability of [6]MCPP within CYP No.3 throughout an extended simulation period of 1  $\mu$ s. Comparable computational analyses confirmed the presence of CPPs within the CYP variants (CYP No.4; Movie S2 for [6]MCPP and S3 for [6]CPP). These computational findings strongly imply the involvement of [6]MCPP-oxylene and [6]CPP-oxylene formation catalyzed by CYP450. Although our calculations successfully demonstrated the binding of [6]MCPP to CYP No.3, this was hindered by the significant spatial separation between the center of [6]MCPP and the active site, namely, heme. In the last MD snapshot, the distance between the center of mass of [6]MCPP and the iron atom of heme was measured to be 14.2 Å, and the nearest neighbor distance from the carbon of [6]MCPP to heme iron was 10.5 Å. Considering the available structural space within CYP No.3 (Figure 4a), we attempted to incorporate an additional [6]MCPP molecule into CYP No.3. Docking and MD simulations confirmed the ability of CYP No.3 to accommodate two [6]MCPP molecules stably (Figure 4b and Movie S4). The time evolution of the distance between [6]MCPP center and heme iron during the MD simulation exhibited an average distance of 10.8 Å with standard deviation of 0.42 Å, and 10.8 Å for the last MD snapshot. The nearest-neighbor distance between the [6]MCPP carbon and heme iron was 6.6 Å. These results substantiate the stable binding of the two [6]MCPP molecules to CYP No.3. Furthermore, our findings demonstrate that the [6]MCPP–heme distance is reduced when two [6]MCPP molecules are introduced, compared to the scenario with only one [6]MCPP molecule. Similar observations were made for the incorporation of two CPP molecules within the CYP No.4 (Movie S5 for two [6]MCPPs and S6 for two [6]CPPs). Thus, our analysis provides substantial evidence supporting the role of CYP450 in the formation of [6]MCPP-oxylene. It is important to note that the MD simulations employed are grounded in classical mechanics and, therefore, cannot elucidate the intricate chemical reaction processes involving the recombination of covalent bonds between atoms.

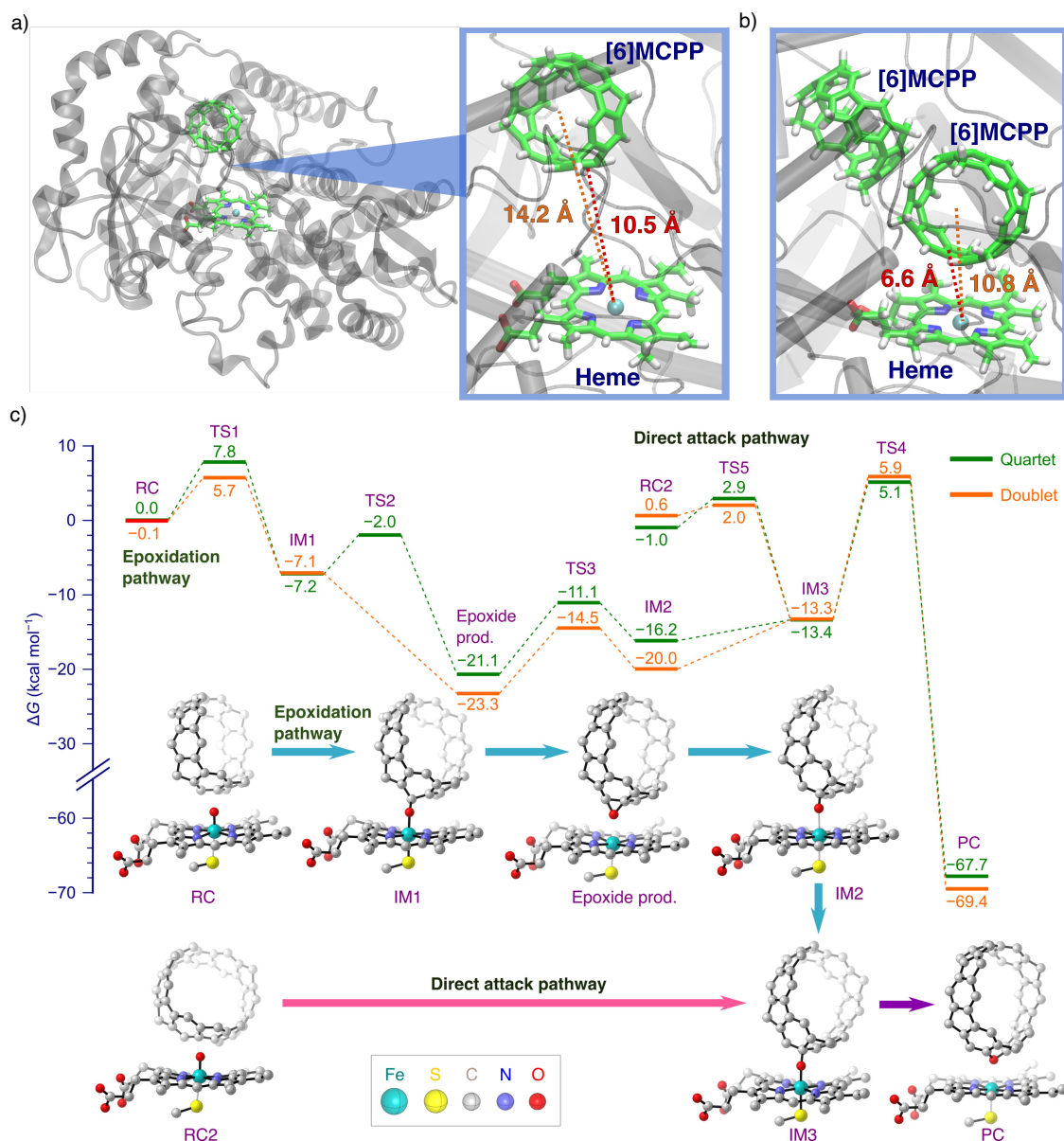


**Figure 4. Substrate binding to CYP variants and mechanism of oxygen-doping.** a) The binding structure of a [6]MCP molecule to CYP No.3 obtained after 1  $\mu$ s of MD simulation. b) Binding structure of the two [6]MCPs to CYP No.3 after 1  $\mu$ s of MD simulation. The distance between the [6]MCP molecular center and Fe atom is shown in orange, and the nearest neighbor distance between the [6]MCP molecule and Fe atom is shown in red. c) Calculated free energy profiles at 298 K for the conversion of [6]MCP to [6]MCP-oxylene catalyzed by Cpd I. Two spin states—quartet and doublet—are considered. Two pathways are proposed: the epoxidation pathway (blue arrows) and the direct pathway (pink arrow). The energy values are expressed in kcal mol<sup>-1</sup>.

### Mechanism of oxygen-doping of [6]MCP

Furthermore, we explored the reaction mechanism for the conversion of [6]MCP to [6]MCP-oxylene, catalyzed by the active species of P450 reaction cycles, Compound I (Cpd I), using Density Functional Theory (DFT) calculations (see Supporting Information for computational details). Our analysis considered two near-degenerate spin states: a quartet and a

doublet.<sup>38</sup> We analyzed two pathways: epoxidation and direct attack (Figure 4c). The epoxidation pathway involved the formation of an intermediate (IM1) and an epoxide product, followed by the formation of two intermediates (IM2 and IM3). The insertion of oxygen into the five-membered ring forms the product. This step is the rate-determining step, with activation free energies from IM2 to TS4 of 25.8 and 21.3 kcal mol<sup>-1</sup> for the doublet and quartet states, respectively. In the direct attack pathway, IM3 was formed directly from a slightly different reactant complex (RC2). The subsequent transformation of IM3 to [6]MCP-oxylene mirrored the epoxidation pathway. We believe that the direct attack pathway is favored over the epoxidation pathway because it involves fewer elementary reactions and has lower activation free energy than the reactant complex. Compared with the epoxide product, the oxylene product was significantly more stable (by more than 45 kcal mol<sup>-1</sup>), indicating that it was the thermodynamic product of the conversion process. We also considered the feasibility of two competing reactions: hydroxylation at either the benzylic or aromatic C–H bonds of [6]MCP. Both products are thermally less stable than the oxylene product by 14.7 and 8.3 kcal mol<sup>-1</sup>, respectively. In addition, for the C–H hydroxylation to be feasible, a linear Fe–O–H arrangement is required. Because of the orientation of [6]MCP relative to Cpd I in the active site, benzylic C–H hydroxylation is expected to be less probable. The formation of the phenol product could theoretically proceed through the non-enzymatic ring opening of the epoxide via protonation, as previously described.<sup>39</sup> However, MD simulations indicated that [6]MCP was stable in the active site, suggesting that the epoxide conversion into phenol was less likely to occur under the studied conditions. We also theoretically explored the formation of [6]MCP-dioxy products by peroxidation (Figure S28). Among three possible dioxy products, the pseudo-*meta* position is the most stable state with a strain energy ( $\Delta H$ ) of 17.4 kcal mol<sup>-1</sup>. However, even when the reaction scale was increased 50-fold, only [6]MCP-oxylene was obtained as the product. Thus, these experimental and computational studies revealed that [6]MCP-oxylene is produced by utilizing a unique biological function.

Finally, the reaction mechanism of the Cpd I-catalyzed conversion of [6]CPP to [6]CPP-oxylene was investigated in a similar manner to the conversion of [6]MCP. The pathways proposed for this reaction (Figures S20 and S21) closely mirror the pathways of [6]MCP. The rate-determining step, exhibiting an activation free energy of ~20 kcal mol<sup>-1</sup>, is still the insertion of oxygen into the [6]CPP ring.

## Conclusions

This study provides insight into the production of single oxygen-doped molecular nanocarbons and the biocatalytic utilization of non-natural molecules. The in-insect synthesis of functional molecular nanocarbons not only offers a new toolbox and opportunity in nanocarbon science, but also represents an immense possibility for biocatalysts in a range of unnatural product syntheses. Although biotransformation reactions present the scientific challenge of high substrate specificity, as demonstrated in this study, we envision that a broader range of molecular nanocarbons can be nonclassically functionalized by utilizing genome-editing technologies to design CYP variants with extended enzyme pockets or mutations in their binding sites. Coupled with the significant recent progress in directed evolution technology and artificial metalloenzymes, the concept of in-insect synthesis offers a unique and alternative option for molecule synthesis, enhancing our ability to discover, develop, and apply unnatural molecules in science and technology, expanding our chemical repertoire.

## REFERENCES

1. Blanco, A.; Blanco, G. Enzymes. *Med. Biochem.* **2017**, 153–175.
2. Robinson, P. K. Enzymes: Principles and Biotechnological Applications. *Essays Biochem.* **2015**, *59*, 1–41.
3. Alissandratos, A. In Vitro Multi-enzymatic Cascades using Recombinant Lysates of *E. coli*: An Emerging Biocatalysis Platform. *Biophys. Rev.* **2020**, *12*, 175–182.
4. Gao, L.; Qiao, H.; Wei, P.; Moussian, B.; Wang, Y. Xenobiotic Responses in Insects. *Arch insect Biochem Physiol.* **2022**, *109*, e21869.
5. Stepek, I. A.; Nagase, M.; Yagi, A.; Itami, K. New paradigms in molecular nanocarbon science. *Tetrahedron* **2022**, *123*, 132907.
6. Scott, L. T.; Boorum, M. M.; McMahan, B. J.; Hagen, S.; Mack, J.; Blank, J.; Wegner, H.; Meijere, A. A rational chemical synthesis C<sub>60</sub>. *Science* **2002**, *295*, 1500–1503.
7. Jasti, R.; Bhattacharjee, J.; Neaton, J. B.; Bertozzi, C. R. Synthesis, Characterization, and Theory of [9]-, [12]-, and [18]Cycloparaphenylene: Carbon Nanohoop Structures. *J. Am. Chem. Soc.* **2008**, *130*, 17646–17647.
8. Takaba, H.; Omachi, H.; Yamamoto, Y.; Bouffard, J.; Itami, K. Selective Synthesis of [12]Cycloparaphenylene. *Angew. Chem. Int. Ed.* **2009**, *48*, 6112–6116.
9. Yamago, S.; Watanabe, Y.; Iwamoto, T. Synthesis of [8]Cycloparaphenylene from a Square-Shaped Tetranuclear Platinum Complex. *Angew. Chem. Int. Ed.* **2010**, *49*, 757–759.
10. Leonhardt, E. J.; Jasti, R. Emerging applications of carbon nanohoops. *Nat. Rev. Chem.* **2019**, *3*, 672–686.
11. Segawa, Y.; Yagi, A.; Matsui, K.; Itami, K. Design and Synthesis of Carbon Nanotube Segments. *Angew. Chem. Int. Ed.* **2016**, *55*, 5136–5158.
12. Povie, G.; Segawa, Y.; Nishihara, T.; Miyauchi, Y.; Itami, K. Synthesis of a carbon nanobelt. *Science* **2017**, *356*, 172–175.
13. Cheung, K. Y.; Gui, S.; Deng, C.; Liang, H.; Xia, Z.; Liu, Z.; Chi, L.; Miao, Q. Synthesis of armchair and chiral carbon nanobelts. *Chem* **2019**, *5*, 838–847.
14. Cheung, K. Y.; Watanabe, K.; Segawa, Y.; Itami, K. Synthesis of a zigzag carbon nanobelt. *Nat. Chem.* **2021**, *13*, 255–259.
15. Han, Y.; Dong, S.; Shao, J.; Fan, W.; Chi, C. Synthesis of a Sidewall Fragment of a (12,0) Carbon Nanotube. *Angew. Chem. Int. Ed.* **2021**, *60*, 2658–2662.
16. Fan, W.; Matsuno, T.; Han, Y.; Wang, X.; Zhou, Q.; Isobe, H.; Wu, J. Synthesis and Chiral Resolution of Twisted Carbon Nanobelts. *J. Am. Chem. Soc.* **2021**, *143*, 15924–15929.
17. Krzeszewski, M.; Ito, H.; Itami, K. Infinitene: A Helically Twisted Figure-Eight [12]Circulene Topoisomer. *J. Am. Chem. Soc.* **2022**, *144*, 862–871.
18. Segawa, Y.; Watanabe, T.; Yamanoue, K.; Kuwayama, M.; Watanabe, K.; Pirillo, J.; Hijikata, Y.; Itami, K. Synthesis of a Möbius carbon nanobelt. *Nat. Synth.* **2022**, *1*, 535–541.

19. Fan, W.; Fukunaga, T. M.; Wu, S.; Han, Y.; Zhou, Q.; Wang, J.; Li, Z.; Hou, X.; Wei, H.; Ni, Y.; Isobe, H.; Wu, J. Synthesis and chiral resolution of a triply twisted Möbius carbon nanobelt. *Nat. Synth.* **2023**, *2*, 880–887 (2023).
20. Li, Y.; Segawa, Y.; Yagi, A.; Itami, K. A Non-alternant Aromatic Belt: Methylene-bridged [6]Cycloparaphenylene Synthesized from Pillar[6]arene. *J. Am. Chem. Soc.* **2020**, *142*, 12850–12856.
21. Kono, H.; Li, Y.; Zanasi, R.; Monaco, G.; Summa, F. F.; Scott, L. T.; Yagi, A.; Itami, K. Methylene-Bridged [6]-, [8]-, and [10]Cycloparaphenylenes: Size-Dependent Properties and Paratropic Belt Currents. *J. Am. Chem. Soc.* **2023**, *145*, 8939–8946.
22. Kawasumi, K.; Zhang, Q.; Segawa, Y.; Scott, L. T.; Itami, K. A grossly warped nanographene and the consequences of multiple odd-membered-ring defects. *Nat. Chem.* **2013**, *5*, 739–744.
23. Lin, H.-A.; Sato, Y.; Segawa, Y.; Nishihara, T.; Sugimoto, N.; Scott, L. T.; Higashiyama, T.; Itami, K. A Water-Soluble Warped Nanographene: Synthesis and Applications for Photoinduced Cell Death. *Angew. Chem. Int. Ed.* **2018**, *57*, 2874–2878 (2018).
24. Kato, K.; Takabe, K.; Maki-Yonemura, S.; Mitoma, N.; Nakahashi, Y.; Nishihara, T.; Hatakeyama, T.; Kawabe, T.; Hijikata, Y.; Pirillo, J.; Scott, L. T.; Yonekura, K.; Segawa, Y.; Itami, K. Double-Helix Supramolecular Nanofibers Assembled from Negatively Curved Nanographenes. *J. Am. Chem. Soc.* **2021**, *143*, 5465–5469.
25. Kaiser, K.; Scriven L. M.; Schulz, F.; Gawel, P.; Gross, L.; Anderson, H. L. An sp-hybridized molecular carbon allotrope, cyclo[18]carbon. *Science* **2019**, *365*, 1299–1301.
26. Gao, Y.; Albercht, F.; Rončević, I.; Etedgui, I.; Kumar, P.; Scriven, L. M.; Christensen, K. E.; Mishra, S.; Righetti, L.; Rossmannek, M.; Tavernelli, I.; Anderson, H. L.; Gross, L. On-surface synthesis of a doubly anti-aromatic carbon allotrope. *Nature* **2023**, *623*, 977–981.
27. Lin, J.; Wang, S.; Zhang, F.; Yang, B.; Du, P.; Chen, C.; Zang, Y.; Zhu, D. Highly efficient charge transport across carbon nanobelts. *Sci. Adv.* **2022**, *8*, eade4692.
28. [https://www.tcichemicals.com/assets/brochure-pdfs/Brochure\\_FF122\\_E.pdf](https://www.tcichemicals.com/assets/brochure-pdfs/Brochure_FF122_E.pdf)
29. Ferry, N.; Edwards, M. G.; Gatehouse, J. A.; Gatehouse, A. M. R. Plant-Insect Interactions: Molecular Approaches to Insect Resistance. *Curr. Opin. Biotechnol.* **2004**, *15*, 155–161.
30. Miyazawa, M.; Takechi, H. Biotransformation of monoterpenoids by the larvae of common cutworm (*Spodoptera litura*). *Nat. Prod. Commun.* **2007**, *2*, 435–443.
31. Cheng, T.; Wu, J.; Wu, J.; Chilukuri, R. V.; Huang, L.; Yamamoto, K.; Feng, L.; Li, W.; Chen, Z.; Guo, H.; Liu, J.; Li, S.; Wang, X.; Peng, L.; Liu, D.; Guo, Y.; Fu, B.; Li, Z.; Liu, C.; Chen, Y.; Tomar, A.; Hilliou, F.; Montagné, N.; Jacquín-Joly, E.; d'Alençon, E.; Seth, R. K.; Bhatnagar, R. K.; Jouraku, A.; Shiotsuki, T.; Kadono-Okuda, K.; Promboon, A.; Smaghe, G.; Arunkumar, K. P.; Kishino, H.; Goldsmith, M. R.; Feng, Q.; Xia, Q.; Mita, K. Genomic adaptation to polyphagy and insecticides in a major east asian noctuid pest. *Nat. Ecol. Evol.* **2017**, *1*, 1747–1756.

32. Marumoto, S.; Okuno, Y.; Hagiwara, Y.; Miyazawa, M. Biotransformation of (+)-Carvone and (-)-Carvone by the Common Cutworm *Spodoptera litura* Larvae. *J. Oleo. Sci.* **2018**, *67*, 1253–1257.
33. Nauen, R.; Zimmer, C. T.; Vontas, J. Heterologous Expression of Insect P450 Enzymes that Metabolize Xenobiotics. *Curr. Opin. Insect. Sci.* **2021**, *43*, 78–84.
34. Wang, R. L.; Xia, Q.; Baerson, S.; Ren, Y.; Wang, J.; Su, Y.; Zheng, S.; Zeng, R. A Novel Cytochrome P450 CYP6AB14 Gene in *Spodoptera litura* (Lepidoptera: Noctuidae) and Its Potential Role in Plant Allelochemical Detoxification. *J. Insect. Physiol.* **2015**, *75*, 54–62.
35. Eberhardt, J.; Santos-Martins, D.; Tillack, A. F.; Forli, S. AutoDock Vina 1.2.0: New Docking Methods, Expanded Force Field, and Python Bindings. *J. Chem. Inf. Model.* **2021**, *61*, 3891–3898.
36. Jumper, J.; Evans, R.; Pritzel, A.; Green, T.; Figurnov, M.; Ronneberger, O.; Tunyasuvunakool, K.; Bates, R.; Židek, A.; Potapenko, A.; Bridgland, A.; Meyer, C.; Kohl, S. A. A.; Ballard, A. J.; Cowie, A.; Romera-Paredes, B.; Nikolov, S.; Jain, R.; Adler, J.; Back, T.; Petersen, S.; Reiman, D.; Clancy, E.; Zielinski, M.; Steinegger, M.; Pacholska, M.; Berghammer, T.; Bodenstein, S.; Silver, D.; Vinyals, O.; Senior, A. W.; Kavukcuoglu, K.; Kohli, P.; Hassabis, D. Highly accurate protein structure prediction with AlphaFold. *Nature* **2021**, *596*, 583–589.
37. Sevrioukova, I. F.; Poulos, T. L. Pyridine-substituted Desoxyritonavir is a More Potent Inhibitor of Cytochrome P450 3A4 than Ritonavir. *J. Med. Chem.* **2013**, *56*, 3733–3741.
38. Phung, Q. M.; Pierloot, K. Low-Lying Electromeric States in Chloro-Ligated Iron(IV)-Oxo Porphyrin as a Model for Compound I, Studied with Second-Order Perturbation Theory Based on Density Matrix Renormalization Group. *J. Chem. Theory Comput.* **2019**, *15*, 3033–3043.
39. de Visser, S. P.; Shaik, S. A Proton-Shuttle Mechanism Mediated by the Porphyrin in Benzene Hydroxylation by Cytochrome P450 Enzymes. *J. Am. Chem. Soc.* **2003**, *125*, 7413–7424.

## ACKNOWLEDGEMENT

We thank Dr. Masahiko Yoshimura (Kyoto University) and Mr. Daiki Imoto (Nagoya University) for fruitful comments. Dr. Issey Takahashi (Nagoya University) is acknowledged for the artworks. K.I. and A.U. thanks JSPS KAKENHI (grant numbers 19H05463 to K.I., and 22K14782 to A.U.), JST ACT-X (grant number JPMJAX22B3 to A.U.), Foundation of Public Interest of Tatematsu (to A.U.), the Sasakawa Scientific Research Grant (to A.U.), the Nakajima Foundation (to A.U.), and the Naito Science & Engineering Foundation (to A.U.), JSPS Promotion of Joint International Research (grant number 22K21346 to A.Y., K.J.F., and T.Y.), and MEXT Promotion of Development of a Joint Usage/Research System Project CURE (grant number JPMXP1323015482 to K.J.F. and T.Y.) for financial support. H.K., H.S., and T.K. thank the Nagoya University Graduate Program of Transformative Chem-Bio Research (WISE Program) supported by MEXT. H.K., H.S. and T.K. thank the JSPS fellowship for young scientists. H.K. thanks the THERS Interdisciplinary Frontier Next Generation Researcher Scholarship supported by MEXT. H.S. thanks the Nagoya University Interdisciplinary Frontier

Fellowship. Computations were performed using the resources of the Research Center for Computational Science, Okazaki, Japan (23-IMS-C087).

**Author contributions:** A.U. and K.I. conceived the concept of in-insect synthesis. K.I. directed the project. A.U. performed all the in-insect synthesis. A.U., H.K., H.Y., and K.A. performed and analyzed biological experiments. A.U., H.K., H.S., T.K., A.Y., and K.I. performed and analyzed synthesis, structure determination, and photophysical property experiments. V.A., Q.M.P., K.J.F., and T.Y. conducted computational studies. All authors analyzed and checked the data. A.U., V.A., K.J.F. and K.I. wrote the manuscript with feedback from other authors. All authors have given approval to the final version of the manuscript.

**Competing interests:** The authors declare no competing interests. No patents were filed.

**Data and materials availability:** Materials and methods, experimental procedures, photophysical studies, NMR spectra, and computational details are available in the Supporting Information or from the corresponding authors upon request. Crystallographic data for the structure of [6]MCP-oxylene and [6]CPP-oxylene are available from the Cambridge Crystallographic Data Centre under reference number 2346752 and 2346751.

### **Supporting Information:**

Materials and Methods

Figures S1 to S29

Tables S1 to S13

Movies S1 to S6

References (S1 to S35)